Vimentin networks at tunable ion-concentration in microfluidic drops

Christian Dammann, Bernd Nöding, and Sarah Köster[a)]
Institute for X-Ray Physics and Courant Research Centre "Nano-Spectroscopy and X-Ray Imaging," Georg-August-Universität Göttingen, 37077 Göttingen, Germany

(Received 27 January 2012; accepted 4 April 2012; published online 18 April 2012)

The structure and function of biological systems, for example, cells and proteins, depend strongly on their chemical environment. To investigate such dependence, we design a polydimethylsiloxane-based microfluidic device to encapsulate biological systems in picoliter-sized drops. The content of each individual drop is tuned in a defined manner. As a key feature of our method, the individual chemical composition is determined and related to the drop content. In our case, the drop content is imaged using microscopy methods, while the drops are immobilized to allow for long-time studies. As an application of our device, we study the influence of divalent ions on vimentin intermediate filament networks in a quantitative way by tuning the magnesium concentration from drop to drop. This way we are able to directly image the effect of magnesium on the fluorescently tagged protein in a few hundreds of drops. Our study shows that with increasing magnesium concentration in the drops, the compaction of the networks becomes more pronounced. The degree of compaction is characterized by different morphologies; freely fluctuating networks are observed at comparatively low magnesium concentrations of 5–10 mM, while with increasing magnesium concentration reaching 16 mM they develop into fully aggregated networks. Our approach demonstrates how a systematic study of interactions in biological systems can benefit from the exceptional controllability of microfluidic methods. © *2012 American Institute of Physics*. [http://dx.doi.org/10.1063/1.4705103]

I. INTRODUCTION

Microfluidic drops have been established as a powerful tool to study chemical and biological systems.[1–5] These applications benefit from the encapsulation of the system of interest inside aqueous drops suspended in an oil phase that act as picoliter-sized compartments, isolating their contents from the surroundings. As a typical feature of microflow studies, these two-phase flow microfluidic experiments provide exceptional controllability and high throughput performance, while keeping the necessary sample volume comparatively small.[6,7] The structure and function of many biological systems that can be studied in these drops, for example, cells, proteins, or multicellular organisms, depend sensitively on parameters such as *p*H, ionic strength, or concentration of certain reagents. Additionally, it is often desirable to investigate biological systems as a function of time, i.e., probe their dynamics. Therefore, a technique that allows for studies of the sensitivity on the environment as well as the time-dependence of biological processes is of high interest. One approach to visualize encapsulated systems in a time-dependent manner is to immobilize the drops by confinement through the channel geometry as introduced by Schmitz *et al.*[8] or by drop trapping using small holes in the channel bottom.[9] Additionally, drops with tunable content can be produced by merging several aqueous components with defined and varying flow speeds.[10] The main problem in combining both approaches consists in knowing the exact contents of each individual drop. In some cases, the chemical of

[a)]Electronic mail: sarah.koester@phys.uni-goettingen.de.

interest can be tagged by a fluorescent label.[11] For enzymatic assays, a fluorogenic substrate can be used to determine the drop contents.[12,13] For other systems, direct fluorescent tagging is not possible (e.g., for small ions) and adding a separate indicating chemical (e.g., a fluorescent dye) could cause unintended crosstalk between the indicating chemical and the encapsulated system, for example, when charged fluorescent dyes interact with proteins. In these cases, we have to rely on the input concentrations to determine the composition of the drops.

Here, we describe an approach to this challenge. We produce drops with varying reagent concentrations, store and image them, and develop a way to preserve the information about the drop content. An advantage of the method is that it requires only syringe pump driven flow and does not need any complex drop manipulation technique like electrical fields. Possible applications of our device in biological or chemical fields are manifold, for instance, protein crystallization,[1,14] cell-based assays,[4,15] or protein network formation.[16,17] As an example for this universal tool, we probe the dependence of network formation of the cytoskeletal intermediate filament (IF) protein vimentin on magnesium ions. It has been shown previously by rheology studies that *in vitro* vimentin filaments build entangled networks that are cross-linked in the presence of divalent ions.[18,19,31] Using microfluidics, we are now in the position to *directly* image the fluorescently labeled networks. We relate the network morphology and density to the magnesium concentration and show that aggregation and compaction of the networks from initially fairly homogeneously distributed, freely fluctuating networks sets on at a magnesium concentration of about 10 mM.

II. MATERIALS AND METHODS

A. Production of microfluidic devices by soft-lithography

Microfluidic devices are produced using PDMS (polydimethylsiloxane) based soft-lithography.[20,21] For this purpose, SU-8 3025 negative resist (MicroChem, Newton, USA) is spin coated onto a silicon wafer to achieve a channel height of 17 μm. PDMS replicas are bonded to standard microscopy cover slips. The devices are stored in Milli-Q water for 1–2 days to saturate the PDMS with water. This step prevents shrinkage of the drops during the experiment. Directly before usage, the devices are flushed with Ombrello (Autoserv, Sinzheim, Germany) to obtain a hydrophobic coating of the channel walls. The devices are connected via polyethylene tubing (Intramedic^{TM} PE20, BD, Franklin Lakes, USA) to gas tight syringes (Hamilton, Bonaduz, Switzerland) which are driven by precise syringe pumps (neMESYS, Cetoni GmbH, Korbußen, Germany). A fluorocarbon oil (Fluorinert^{TM} FC-40, 3 M Deutschland GmbH, Neuss, Germany) is used as the oil phase of the emulsion. A perfluoropolyether-polyethyleneglycol block-copolymer surfactant (Raindance Technologies, Lexington, USA) is added at a concentration of 1.8% (w/w) to stabilize the emulsion and, at the same time, ensure bio-compatibility.[22]

B. Protein purification, labeling, and assembly

Human vimentin protein is expressed in *Escherichia coli* bacteria and then purified from inclusion bodies.[23] Vimentin is stored at −80 °C in 8 M urea, 5 mM Tris-HCl (*p*H 7.5), 1 mM ethylene diamine tetraacetic acid, 0.1 mM ethylene glycol tetraacetic acid, 1 mM dithiothreitol, and 10 mM methyl ammonium chloride (MAC). The protein is fluorescently tagged using AlexaFluor 488 C_5 Maleimide (Invitrogen GmbH, Darmstadt, Germany).[24] Labeled and unlabeled vimentin are mixed at a ratio of 3:2 to achieve optimized assembly kinetics and imaging properties. After mixing, vimentin is dialyzed against 6 M urea, 0.8 mM phosphate buffer for 1 h, and subsequently two times against 2 mM phosphate buffer, first for 1 h and then over night. The protein is assembled into filaments at a concentration of 600 μg/ml in 100 mM KCl (*p*H 7.5), 2 mM phosphate buffer at 37 °C for approximately 15 h and is used directly afterwards. At this chosen input concentration, the protein networks can nicely be imaged in the drops. This assembly procedure leads to a broad distribution of filament lengths with an average contour length of about 10 μm.[25]

C. Long-time imaging of vimentin in drops

We study vimentin network formation in drops in dependence of the magnesium concentration ($c_{Mg^{2+}}$). For these experiments, we choose a magnesium component (31 mM $MgCl_2$,

100 mM KCl, and 2 mM phosphate buffer) referred to as "aqueous 1," a buffer component (100 mM KCl and 2 mM phosphate buffer) referred to as "aqueous 2," and a vimentin component (600 μg/ml vimentin, 100 mM KCl, and 2 mM phosphate buffer) referred to as "aqueous 3" (see Fig. 1). Vimentin protein networks are encapsulated in microfluidic drops as will be described below. The drops are immobilized in the microfluidic device which is placed in an on-stage incubation chamber (INUG2E-ONICS, Tokai Hit CO., Ltd., Fujinomiya-shi Shizuoka-ken, Japan) during the imaging period. The incubation chamber provides a water saturated atmosphere that prevents the initially water-saturated PDMS from drying out. By this means, the drop volume is preserved for several hours. Additionally, the chamber keeps the microfluidic device at roughly 37 °C. The incubation chamber is mounted on an inverted microscope (IX 81, Olympus, Hamburg, Germany) equipped with a 40x oil immersion objective (UPlanFLN, Olympus), an Olympus CellR setup for widefield fluorescence microscopy, and a sensitive camera (Hamamatsu Orca-R2 for imaging of protein networks and PCO.edge for imaging of fluorescein filled drops). Using this setup, the whole drop series is imaged within the first 2 h after the protein is encapsulated in drops.

III. RESULTS

A. The microfluidic device

The microfluidic device in which the picoliter water drops are composed, collected, and prepared for long-time storage is illustrated in Fig. 1. This PDMS-based device follows a modular design concept that enables drop manipulation at high accuracy by changing flow rates only. For a tunable composition of the drop content, the default setup contains three aqueous inlet channels that join up in the *drop composer* in a side-by-side flow at low Reynolds number conditions

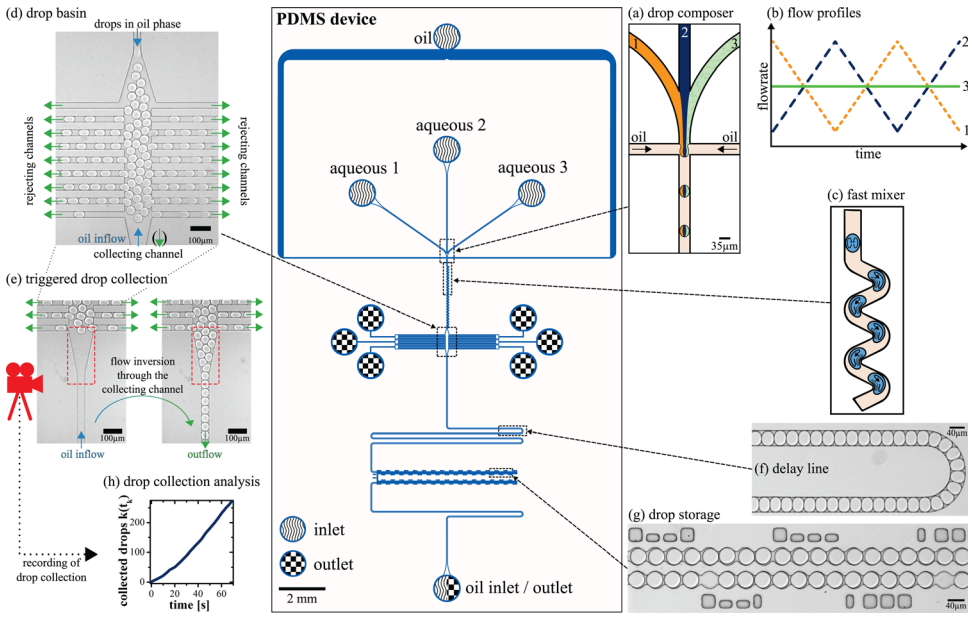

FIG. 1. The microfluidic device. (a) In a PDMS-based microfluidic device three aqueous components are merged together, (b) while the flow rates of two of them are alternated in a periodic way. This way microfluidic drops with tunable content are produced in a flow focusing channel design. (c) The drops pass a serpentine channel that ensures fast mixing of the drop content which is due to the recirculating flow and chaotic advection within the moving drops. (d) In a *drop basin*, the drops are densified and excess drops are rejected to six outlet channels. At the bottom of the basin, there is a connection to a long channel which is called *collecting channel*. (e) At first, oil flows through this collecting channel into the basin so that no drop can enter. The inversion of the flow direction of the oil through the collecting channel triggers the collection of the drops in a controlled manner. (h) To determine the drop content afterwards, the drop collection process is recorded. (f) The first part of the collecting channel is a *delay line* which ensures smooth drop collection. (g) Finally, the drops reach the *drop storage* which is a region with constrictions at the channel walls.[8] Due to this confinement, the drops are immobilized when the overall flow rates in the device are stopped.

(Fig. 1(a)).[6] This design enables us to supply one aqueous component "3" at a constant flow rate. For example, this component can be a protein solution so that the protein concentration in all drops is kept constant. For the remaining two aqueous components, periodic and triangularly shaped pump profiles are chosen that oppose each other (Fig. 1(b)). This way, the overall flow rate of the aqueous phase remains constant, while the concentration of one reagent is varied. For instance, the salt concentration in the drops is varied when the pump profiles of a buffer A as aqueous component "2" and the buffer A with added salt (aqueous component "1") oppose each other.

Shortly after the three aqueous components join up they reach a flow focusing channel geometry[6] in the drop composer where the composite aqueous phase is focused laterally by an oil phase. By default, a mean total flow velocity of 14 mm s^{-1} for the aqueous phase and 23 mm s^{-1} for the oil phase is used, which leads to monodisperse and oblate drops, approximately 40 μm in diameter and 17 μm in height. These drops act as isolated containers for the encapsulated aqueous phase. To overcome the slow (on the order of seconds) diffusive mixing in the side-by-side flow pattern of the aqueous components, the drops are directed to a serpentine channel with narrow windings. This serpentine channel ensures a rapid content mixing on the order of milliseconds. This fast mixing is achieved through the recirculating flow in the moving plug-like drop and further enhanced through chaotic advection induced by the windings (Fig. 1(c)).[26]

The serpentine channel ends in a wider multi-way channel system which we refer to as *drop basin* (Fig. 1(d)). The majority of the channels that end in this basin are located laterally and conduct the fluid towards outlets where it is disposed of. Drops are produced at a rate of approximately 400 Hz, but only a few hundred drops are stored further downstream the device, ideally spread out over a period of time of at least 10 s. The drop basin serves the purpose to reject a large portion of the incoming drops. By rejecting a large portion of the drops, we increase the accuracy with which the concentration gradient from drop to drop is being established. Additionally, it densifies the drops by removing excess oil, since the oil of the two-phase flow is filtered out more easily than the drops (Fig. 1(d)). This densification is important for an efficient drop storage later on. One more channel is located at the bottom of the drop basin: the *collecting channel*. At first, oil flows through the collecting channel into the basin preventing any drops from entering this channel. At the onset of drop collection for storage, we invert the oil flow direction through the collecting channel, i.e., change the mean flow velocity from +4 mm s^{-1} to −2 mm s^{-1}.

After a delay of about 1 min this leads to the collection of a statistical fraction of the drops into the collecting channel at a rate of about 5 Hz (Fig. 1(e)). Owing to the fact that only three drops can flow side-by-side in the basin and all drops on the left and right hand sides are rejected (data not shown), the order of the statistically collected drops remains chronological throughout the whole drop collection process. In total, about 1 out of 80 drops is kept and not rejected. One minute collection time provides a sufficiently large number of drops. This collection is recorded using brightfield microscopy to determine the drop content later on (see Sec. III B). We then take the syringe that supplies the collecting channel with oil out of the syringe pump and operate it manually in the remaining steps which is more accurate than using the pumps in this case. In parallel to this manual operation, we observe the drop flow through the eyepiece of the microscope. This way the drops are conducted into a region with circular constrictions at the channel walls. These circular shapes correspond to the most stable shape of the drops (Fig. 1(g)).[8] When we stop the flow in the entire device, the drops are stored and can be imaged in this *drop storage* for several hours.

Since the drop storage is designed to host a few hundreds of drops during one experiment and all circular storing positions look the same, it is necessary to label them uniquely. Therefore, we add a numeral code next to the storage sites to identify clusters of eight drops (Fig. 1(g)). In this code, we provide numbers to the basis of 3 using a vertical bar, a horizontal bar, and a square. These simple shapes can easily be reproduced by soft-lithography.

B. Determination of the drop content

One challenge in multiplexing experiments by using drop microfluidics is to determine the precise chemical composition of the drop contents. To do so, the delay time t_d between the

input pump profile and the actual moment of drop collection has to be taken into account as well as possible changes to the input profile due to damping effects of the elastic microfluidic device material.

To access both aspects and characterize the device thoroughly, we first perform experiments with varying fluorescein concentrations c_{Fl} over a drop series and determine the resulting fluorescence intensity in each drop when it enters the collecting channel. The fluorescein concentration is directly determined from the measured intensities based on the calibration measurements. The input and measured fluorescein concentrations as a function of time for a typical experiment are shown in Fig. 2(a). The input fluorescein concentration is calculated based on the knowledge of the fluorescein concentration in the syringe (100 μM, "aqueous 1" in Fig. 1) and the flow rates of the aqueous components when we apply a triangular pump profile with a periodicity of 15 s (Fig. 1(b)). Note that while the signal (e.g., c_{Fl}) versus drop number k is not strictly periodic, it actually is when translated to the time domain. The comparison in Fig. 2(a) shows that the periodicity and the mean values of the curves agree well. However, very high and very low fluorescein concentrations are not reached experimentally, likely due to the elastic device materials and inertial effects when changing pump speeds. The triangular input concentration profile (violet stars) leads to a sine-shaped profile of fluorescein concentration in the measured drops (green circles) and is fitted accordingly to retrieve a calculated and calibrated

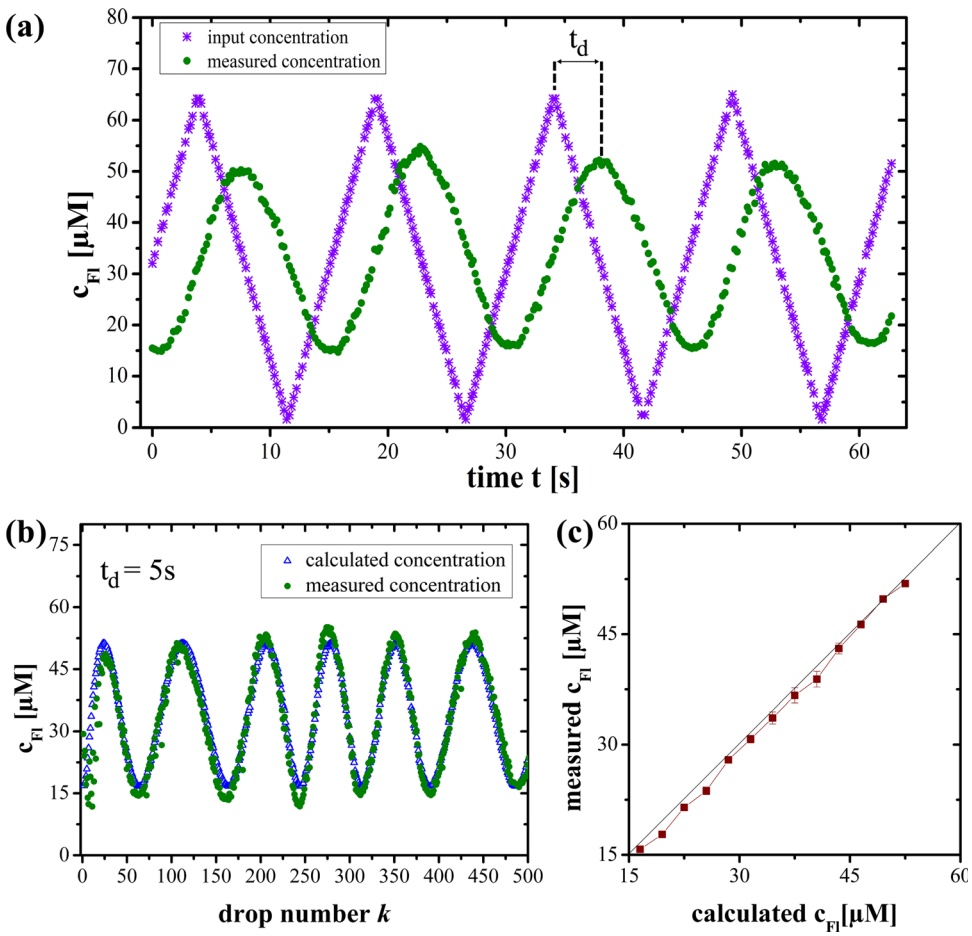

FIG. 2. Determination of the fluorescein concentration in a drop series. (a) Comparison of the input and measured fluorescein concentration in drops as a function of time. Using triangular input pump profiles (violet stars), the measured concentration profile in the drops has the shape of a sine function (green circles). (b) The delay time t_d is determined by a regression method. The measured (green circles) and calculated (blue triangles) concentrations in the drops agree well. (c) Measured fluorescein concentration (bins of 3 μM width) plotted over the calculated values. The straight line has a slope of 1. Error bars are not shown when smaller than symbols.

concentration on the basis of several independent experiments. This calibration curve which translates the input flow profile to the actually measured concentrations in the drops is used in the following experiments.

As a proof of principle and before moving to drop contents that cannot directly be imaged (magnesium ions, see Sec. III C), we apply the calibration as described in the previous paragraph to a separate fluorescein experiment. The time shift between the input and the measured concentrations as given by t_d in Fig. 2(a) has to be taken into account as well as the sine-shape of the flow rate profile $Q(t)$. Considering both factors, the fluorescein concentration of the kth drop in the series is given by

$$c_{Fl}(t_k) = \frac{c_{syr}}{Q_{aq}} \times Q(t_k - t_d), \tag{1}$$

where c_{syr} is the fluorescein concentration in the syringe, Q_{aq} ($30\,\mu l\,h^{-1}$ in our case) is the overall flow rate of the aqueous phase, and t_k is the time when the kth drop is collected. t_k is directly obtained from the analysis of the drop collection video (Fig. 1(h)). Thus, the calculated and the measured fluorescein concentrations agree well, showing the validity of the method. Nevertheless, the fit can even be improved. To do so, we group the drops into bins of similar concentration (3 μM width), average the concentrations within the bins and plot this average together with its error δ_i as a function of the calculated concentration. By minimizing the total error $\sum_i \delta_i$, we determine the best match of the two concentration curves (Figs. 2(b) and 2(c)). For the first drops ($\approx 1-20$), we observe deviations which are likely due to bleaching effects of the fluorescein in the first slowly moving drops. For the remaining drops, the measured and calculated values agree well.

After having successfully tested the calibration on the fluorescein measurement, we will apply the same method to experiments on vimentin networks in the presence of varying magnesium concentrations in drops in Sec. III C. Again, the calibration curve derived from the data shown in Fig. 2(a) and similar experiments are used followed by error minimization. In this case, we use the network morphology as the "characteristic signal" (which depends on the magnesium concentration) for each drop instead of fluorescein concentration as discussed in this section. This method allows us to determine the composition of each vimentin-filled drop, although the composition (i.e., the magnesium concentration) cannot be directly measured.

C. Vimentin networks in picoliter drops

One central question in cell mechanics is how network formation of biopolymers and crosslinking is mediated by multivalent ions or specific binding molecules. Here, we study the influence of divalent magnesium ions on the vimentin IFs. To do so, we produce, store, and observe a drop series, each drop containing the same amount of protein, the same buffer conditions, but successively varied magnesium concentration. The resulting vimentin networks are imaged by fluorescence microscopy. Depending on the magnesium concentration in an individual drop, we observe qualitatively different network morphologies (Fig. 3, top). We analyze the fluorescence intensity distribution taken over the entire drop (circles in Fig. 3) to quantitatively characterize these different network morphologies. We normalize the overall fluorescence intensity in each drop and describe the morphologies by the standard deviation σ of the intensity distribution.[16] This concept is illustrated in Fig. 3, bottom, where we compare the standard deviation of a freely fluctuating network (a), an aggregated network (b), and a fully compacted network (c). The degree of aggregation and compaction of these networks increases from (a) to (c), and the standard deviation increases as well. This effect can be understood considering the volume that is occupied by the fluorescing aggregates in the drop. The intensity variability is small in the rather homogeneous fluorescence intensity in a drop with freely fluctuating networks; consequently, the standard deviation is small. By contrast, in the case of a fully compacted network only a small part of the drop area shows a high intensity, whereas the rest of the drop shows very little fluorescence. Accordingly, this leads to a large standard deviation of the intensity distribution.

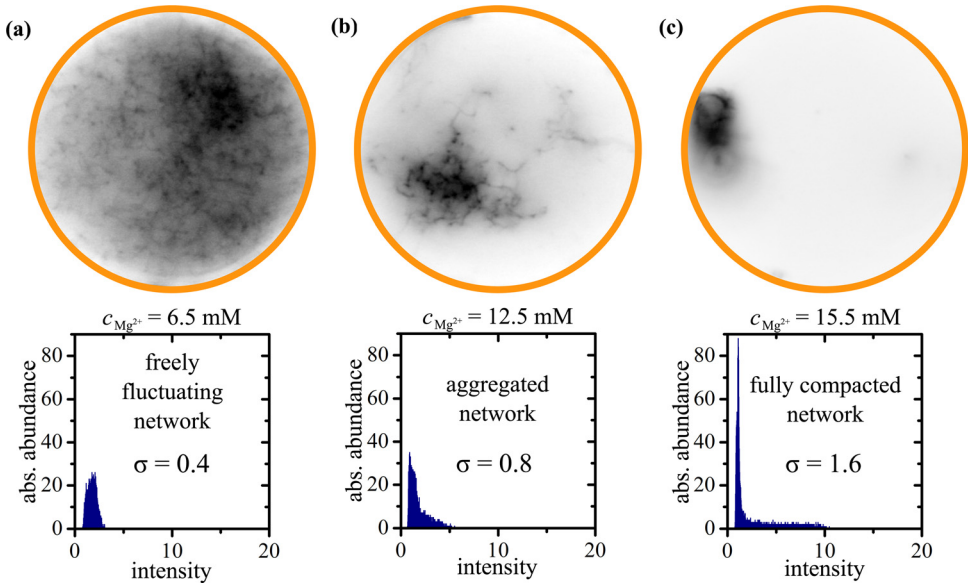

FIG. 3. Vimentin networks in drops. Top: fluorescence micrographs (inverted gray scale, adjusted for displaying purposes) of vimentin networks at different magnesium concentrations $c_{Mg^{2+}}$. Bottom: intensity histograms of the fluorescence micrographs (total fluorescence intensity in each drop normalized to 10^5). Different network morphologies result in different standard deviations σ of the fluorescence intensity distribution: (a) Freely fluctuating networks show a narrow distribution, since the overall intensity is comparatively homogeneous. (b) The distribution of networks that have aggregated is broader leading to a higher value for σ. (c) Networks that are fully compacted to an intensely fluorescing aggregate show the largest standard deviation. The drop diameters are 40 μm.

We analyze the standard deviation σ of vimentin networks for about 250 drops per experiment. The values for σ give us a "signal" for each drop in the series, which we show exemplarily in Fig. 4(a) (green solid circles). Additionally, we determine the magnesium concentration $c_{Mg^{2+}}$ for each drop of the same series (blue open triangles) based on the calibration using fluorescein. The data are binned (1 mM $c_{Mg^{2+}}$ intervals), and the averaged standard deviation $\bar{\sigma}$ is shown as a function of the magnesium concentration in Fig. 4(b) (green squares and magenta circles). We find an almost constant value for $\bar{\sigma}$ for $c_{Mg^{2+}} = 5\ldots10$ mM indicating that in this range, the networks are homogeneous and freely fluctuating. Starting from a threshold of $c_{Mg^{2+}} \approx 10$ mM, $\bar{\sigma}$ increases significantly as $c_{Mg^{2+}}$ increases. The region around 10 mM is shown for smaller bin sizes in Fig. S1, see supplementary material.[27] From this analysis, we deduce that an increase of $c_{Mg^{2+}}$ induces the compaction of vimentin networks. The higher

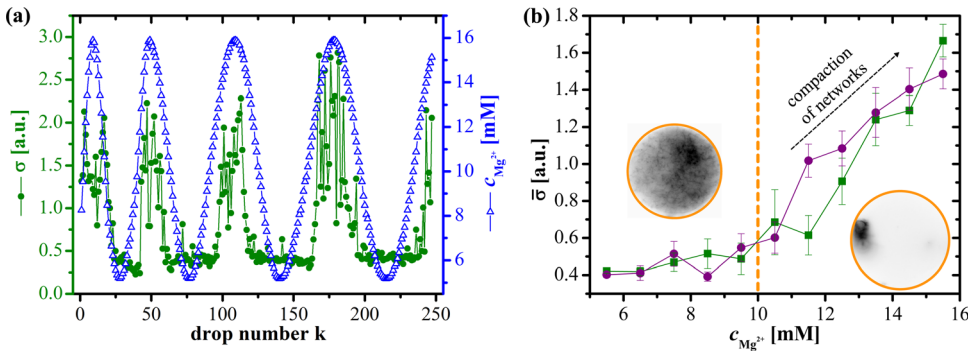

FIG. 4. Dependence of vimentin network morphology on the magnesium concentration. (a) For a vimentin-containing drop series, the standard deviation σ of the gray scale values is compared to the magnesium concentration for each drop. (b) Binning of the results (1 mM $c_{Mg^{2+}}$ intervals) leads to an averaged standard deviation $\bar{\sigma}$ as a function of $c_{Mg^{2+}}$, shown here for two independent experiments. These curves show the ability of magnesium to induce network compaction of vimentin networks.

$c_{Mg^{2+}}$ is, the higher is the degree of network compaction. Since networks with $\bar{\sigma} \approx 1.6$ are already highly condensed in the drop (Fig. 3(c)), we expect that vimentin networks cannot be compacted much further at higher $c_{Mg^{2+}}$ than we apply in the experiment. Therefore, $c_{Mg^{2+}} = 16\,\text{mM}$ is assumedly a concentration at which the network condensation is fairly saturated. As shown in Fig. 4(b), the results for two independent experiments agree very well. Importantly, the onset of network aggregation and compaction is found at $c_{Mg^{2+}} \approx 10\,\text{mM}$ in both cases.

IV. DISCUSSION AND CONCLUSION

We demonstrate the concentration determination of a solute that we vary over a series of microfluidic drops for the general case where the solute cannot be directly visualized (e.g., small ions). We use the response of the system (protein networks) to determine the concentration of the solute (magnesium ions). To quantify the different occurring network morphologies, we determine the standard deviation of the gray scale histograms from the fluorescence micrographs. The method we demonstrate here on the example of protein networks in the presence of ions can be applied to any other system that responds to a chemical at a concentration c with a specific signal $s(c)$. In the example, we show here $s(c)$ is a monotonic function. However, in principle $s(c)$ can be arbitrary, since the regression method we use to determine the delay time t_d does not take into account any specific course of $s(c)$. Consequently, the method could also be applied for the study of many other systems, where the influence of a reagent on a biological system, be it multicellular organisms, single cells, or cellular components, shall be investigated. The modular design employing only syringe pump driven flow (no electrical fields or there like) renders the device a stable and easy-to-use solution for many applications.

A straightforward approach to study the network formation of fluorescently labeled vimentin as a function of magnesium concentration would be to prepare the solutions in bulk and image the resulting networks on a cover slip. However, this proves to be difficult. A filament network is a three dimensional construct and imaging it on a two dimensional cover slip distorts the results. Therefore, microfluidic drops that are stabilized with a biocompatible surfactant are an ideal tool to avoid interactions with an interface. Moreover, preparing hundreds of nearly identical samples with only one parameter varied (in our case the magnesium concentration) is a tedious and almost impossible task; either an assay with high dosing precision can be prepared consuming high sample volumes or the assay is prepared at low sample volumes, sacrificing dosing precision. Drop microfluidics provides both low sample consumption (minimum protein volume for the total experiment 20 μl) as well as high dosing precision owing to the controllability of the method. Using the device once, we obtain data for a few hundred individual "mixtures" considering each drop separately. This provides data for good statistics. Immobilization of the drops in the drop storage also allows for time-lapse studies of individual networks in certain drops. Constriction to a drop volume of 20 pl mimics the cellular confinement that cytoskeletal proteins encounter in the cytosol surrounded by the cell membrane.

Analyzing the directly imaged vimentin networks in microfluidic drops, we find a compacting influence of magnesium ions on vimentin aggregates at a protein concentration of 200 μg/ml. This influence becomes apparent for magnesium concentrations of about 10 mM and higher. As a consequence of this compaction, the total volume occupied by vimentin in the drops decreases as the magnesium concentration increases. At the same time, the fluorescence intensity per volume of the compacted network increases.

It was found in rheology experiments that magnesium ions act as effective cross-linkers of vimentin networks.[18,19,31] Our results are consistent with these findings considering that cross-linkers densify a network, and our study shows the compacting influence of magnesium ions. In the rheology studies, the vimentin concentration is about one order of magnitude higher than in the work presented here, and the onset of cross-linking is observed at lower magnesium concentrations; the ratios of magnesium to protein concentrations range between $R = c_{Mg^{2+}}/c_{vim} = 105$ and $R = 215$. Interestingly, electron micrographs of the networks do not show a morphological difference of these cross-linked networks as compared to entangled networks without cross-linking.[31] Here, we increase the relative magnesium concentration further and systematically

cover the range from $R = 1300$ to $R = 4200$. We observe the onset of compaction at $R \approx 2600$. We assume that apart from the relative concentration of magnesium and the absolute protein concentration, time is an important factor in network formation and compaction. A time-resolved study of networks in drops would therefore be a logic next step in order to investigate this dependence.

At very high ion concentrations (see Fig. 3(c)), the vimentin aggregates have a diameter of about 9 μm. Taking into account that vimentin IFs have a persistence length on the order of 1 μm,[28–30] we can assume that a further densification would be hindered by the intrinsic stiffness of the filaments. Assuming that all the protein in the drop is compacted to the aggregate, the local vimentin concentration is estimated to 10 mg/ml. At this high value, a further densification might also be sterically hindered.

To conclude, our experiments on vimentin with added magnesium demonstrate the exceptional experimental controllability provided by the developed microfluidic device. We are able to precisely tune and determine the contents of the drops and can vary them drop by drop, providing a platform for multiple experiments at once. The combination with fluorescence microscopy allows us to directly image the drop content, in our case individual protein networks. The device is not restricted to the application presented here but can be used to study varying biological or non-biological systems that react to parameters of its environment, such as ionic strength, reagent concentration, or *p*H. Additionally the small and easily manageable microfluidic chip allows for the convenient variation of external parameters such as temperature. We expect manifold uses of this kind of device also in other fields of research.

ACKNOWLEDGMENTS

We would like to thank Harald Herrmann for fruitful discussions, Susanne Bauch and Jens-Friedrich Nolting for technical assistance and Brian Hutchison for providing the surfactant. This work was supported by the German Research Foundation (DFG) in the framework of SFB 755, CMPB and the Excellence Initiative.

[1]H. Song, D. L. Chen, and R. F. Ismagilov, Angew. Chem., Int. Ed. **45**, 7336 (2006).
[2]A. B. Theberge, F. Courtois, Y. Schaerli, M. Fischlechner, C. Abell, F. Hollfelder, and W. T. S. Huck, Angew. Chem., Int. Ed. **49**, 5846 (2010).
[3]D. T. Chiu and R. M. Lorenz, Acc. Chem. Res. **42**, 649 (2009).
[4]S. Köster, F. E. Angilè, H. Duan, J. J. Agresti, A. Wintner, C. H. J. Schmitz, A. C. Rowat, C. A. Merten, D. Pisignano, A. D. Griffiths, and D. A. Weitz, Lab Chip **8**, 1110 (2008).
[5]J. Clausell-Tormos, D. Lieber, J.-C. Baret, A. El-Harrak, O. J. Miller, L. Frenz, J. Blouwolff, K. J. Humphry, S. Köster, H. Duan, C. Holtze, D. A. Weitz, A. D. Griffiths, and C. A. Merten, Chem. Biol. **15**, 427 (2008).
[6]S. L. Anna, N. Bontoux, and H. A. Stone, Appl. Phys. Lett. **82**, 364 (2003).
[7]M. Joanicot and A. Ajdari, Science **309**, 887 (2005).
[8]C. H. J. Schmitz, A. C. Rowat, S. Köster, and D. A. Weitz, Lab Chip **9**, 44 (2009).
[9]P. Abbyad, R. Dangla, A. Alexandrou, and C. N. Baroud, Lab Chip **11**, 813 (2011).
[10]H. Song and R. F. Ismagilov, J. Am. Chem. Soc. **125**, 14613 (2003).
[11]J.-C. Baret, Y. Beck, I. Billas-Massobrio, D. Moras, and A. D. Griffiths, Chem. Biol. **17**, 528 (2010).
[12]J. J. Agresti, E. Antipov, A. R. Abate, K. Ahn, A. C. Rowat, J.-C. Baret, M. Marquez, A. M. Klibanov, A. D. Griffiths, and D. A. Weitz, Proc. Natl. Acad. Sci. U.S.A. **107**, 4004 (2010).
[13]A. Huebner, L. F. Olguin, D. Bratton, G. Whyte, W. T. S. Huck, A. J. de Mello, J. B. Edel, C. Abell, and F. Hollfelder, Anal. Chem. **80**, 3890 (2008).
[14]J. U. Shim, G. Cristobal, D. R. Link, T. Thorsen, and S. Fraden, Cryst. Growth Des. **7**, 2192 (2007).
[15]E. Brouzes, M. Medkova, N. Savenelli, D. Marran, M. Twardowski, J. B. Hutchison, J. M. Rothberg, D. R. Link, N. Perrimon, and M. L. Samuels, Proc. Natl. Acad. Sci. U.S.A. **106**, 14195 (2009).
[16]H. M. Evans, E. Surenjav, C. Priest, S. Herminghaus, R. Seemann, and T. Pfohl, Lab Chip **9**, 1933 (2009).
[17]M. M. A. E. Claessens, M. Bathe, E. Frey, and A. R. Bausch, Nature Mater. **5**, 748 (2006).
[18]S. Köster, Y.-C. Lin, H. Herrmann, and D. A. Weitz, Soft Matter **6**, 1910 (2010).
[19]Y.-C. Lin, N. Y. Yao, C. P. Broedersz, H. Herrmann, F. C. MacKintosh, and D. A. Weitz, Phys. Rev. Lett. **104**, 058101 (2010).
[20]S. R. Quake and A. Scherer, Science **290**, 1536 (2000).
[21]D. Duffy, J. McDonald, O. Schueller, and G. Whitesides, Anal. Chem. **70**, 4974 (1998).
[22]C. Holtze, A. C. Rowat, J. J. Agresti, J. B. Hutchison, F. E. Angilè, C. H. J. Schmitz, S. Köster, H. Duan, K. J. Humphry, R. A. Scanga, J. S. Johnson, D. Pisignano, and D. A. Weitz, Lab Chip **8**, 1632 (2008).
[23]H. Herrmann, L. Kreplak, and U. Aebi, in *Intermediate Filament Cytoskeleton, Methods in Cell Biology*, edited by M. B. Omary and P. A. Coulombe (Academic, 2004), Vol. 78, pp. 3–24.

[24]S. Winheim, A. R. Hieb, M. Silbermann, E.-M. Surmann, T. Wedig, H. Herrmann, J. Langowski, and N. Mücke, PLoS ONE **6**, e19202 (2011).
[25]S. Portet, N. Mücke, R. Kirmse, J. Langowski, M. Beil, and H. Herrmann, Langmuir **25**, 8817 (2009).
[26]M. R. Bringer, C. J. Gerdts, H. Song, J. D. Tice, and R. F. Ismagilov, Philos. Trans. R. Soc. London, Ser. A. **362**, 1087 (2004).
[27]See supplementary material at http://dx.doi.org/10.1063/1.4705103 for a close-up of the network condensation threshold around 10 mM magnesium.
[28]N. Mücke, L. Kreplak, R. Kirmse, T. Wedig, H. Herrmann, U. Aebi, and J. Langowski, J. Mol. Biol. **335**, 1241 (2004).
[29]M. Schopferer, H. Bär, B. Hochstein, S. Sharma, N. Mücke, H. Herrmann, and N. Willenbacher, J. Mol. Biol. **388**, 133 (2009).
[30]B. Nöding and S. Köster, Phys. Rev. Lett. **108**, 088101 (2012).
[31]Y.-C. Lin, C. P. Broedersz, A. C. Rowat, T. Wedig, H. Herrmann, F. C. MacKintosh, and D. A. Weitz, J. Mol. Biol. **399**(4), 637–644 (2010).